Pseudopotentials for the calculation of dynamic properties of liquids

2001 J. Phys.: Condens. Matter 13 7801

(http://iopscience.iop.org/0953-8984/13/34/321)

INSTITUTE OF PHYSICS PUBLISHING JOURNAL OF PHYSICS: CONDENSED MATTER

J. Phys.: Condens. Matter **13** (2001) 7801–7825 PII: S0953-8984(01)26870-2

Pseudopotentials for the calculation of dynamic properties of liquids

L E González, D J González and J M López

Departamento de Física Teórica, Universidad de Valladolid, Valladolid, Spain

Received 12 July 2001
Published 9 August 2001
Online at stacks.iop.org/JPhysCM/13/7801

Abstract

The calculation of dynamic properties of physical systems requires the knowledge of their total energy as a function of their configuration. In this paper we review some techniques for making this evaluation feasible in liquid systems, in particular liquid metals, through the use of pseudopotentials, and we also discuss how to construct the pseudopotentials in order to optimize their use within approximate theories for the total energy. Some results are given for pure metals and alloys.

1. Introduction

From a fundamental point of view, ordinary matter is composed by atomic nuclei and electrons interacting through electromagnetic forces. However, in many situations it is enough to consider just electrostatic Coulomb interactions to obtain an accurate description of a physical system. Furthermore, in atoms, molecules, and also condensed matter phases, the electrons can be divided into two categories: those tightly bound to the nucleus, referred to as *core* electrons, and the others, not so tightly bound, which will be referred to as *valence* electrons. When the environment of an atom changes, perhaps because of the presence of other interacting atoms, the state of the valence electrons also changes, in some cases drastically (for instance in a metal), whereas the core electrons are hardly affected and therefore in most cases they can be considered to be chemically inert. Consequently, most properties of matter depend only on the behaviour of the chemically active valence electrons.

The preceding argument shows that the potential felt by the valence electrons in a given system plays a basic role in the determination of its properties. In fact, it is a rather peculiar potential with a complicated behaviour in the core regions because of the interaction with the nucleus and with the core electrons; moreover it diverges at the nuclear position due to the nuclear attraction. On the other hand, the valence wavefunctions must oscillate inside the core region, since they must be orthogonal to the core wavefunctions. This strong and complicated character of the potential in the core region makes it rather difficult to perform accurate calculations. Fortunately, most properties do not depend very strongly on this complicated behaviour, because the important interaction among the different atoms of the

system takes place where their valence wavefunctions overlap, and this is certainly outside the core regions. So, it happens that the problematic core region is not really important for the properties of interest.

The situation is made more tractable by introducing the so-called pseudopotential. This is a potential which, in a certain sense, is *equivalent* to the real potential felt by the valence electrons outside the cores, but which behaves very differently from the real potential inside the core regions. In general, the pseudopotential is intended to be *weak* enough that it does not bind any core electrons. In particular, close to the nucleus it will not be Coulombic any more; moreover, as there are no core electrons, the corresponding wavefunctions (i.e., the pseudowavefunctions) are smooth within the core, with no rapid oscillations, as opposed to the true valence wavefunctions. The weakness of the pseudopotential and the smoothness of the pseudowavefunctions are very convenient, for instance, in a perturbative calculation of the total energy of a system, or in a calculation of the electronic states via an expansion in a series of plane waves. On the other hand, the pseudopotential is constructed so as to have the same energy spectrum as the true potential (except for the core states) with the same scattering properties, and to give the same valence pseudowavefunctions as the true potential in the region outside the cores (this is the meaning of the *equivalence* mentioned before).

These convenient properties of the pseudopotential are however somewhat outweighed by its relative complexity. In its more general form, the pseudopotential is represented by a non-local and energy-dependent operator. For instance, the orthogonalized plane-wave (OPW) pseudopotential [1] acts on a wavefunction as

$$V_{\mathrm{ps}}^{\mathrm{OPW}}|\psi\rangle = \mathcal{V}|\psi\rangle + \sum_{nlm;i}(E - E_{nlm;i})|\psi_{nlm;i}\rangle\langle\psi_{nlm;i}|\psi\rangle$$

where $\mathcal{V}$ is the true potential felt by the electrons, and $|\psi_{nlm;i}\rangle$ and $E_{nlm;i}$ are the core wavefunctions and energies with quantum numbers n, l, and m for the ion at position $\vec{R}_i$.

The OPW method is a rather standard method for computing the band structure of a solid [1], where the valence band energies are obtained by diagonalization of the true Hamiltonian (i.e. the one that includes the true crystal potential $\mathcal{V}$), which is represented in a basis set formed by functions called orthogonalized plane waves. However, it was realized that these energies could also be interpreted as those obtained through the diagonalization of the OPW pseudo-Hamiltonian (i.e. that including the OPW pseudopotential) represented in the standard plane-wave basis set. Actually, this was the historical origin of the development and use of pseudopotentials, in particular for the studies of metals.

In fact, the OPW expression for the pseudopotential is quite complicated, because of the appearance of the true potential; moreover it describes the crystal potential. Later on, simpler expressions were proposed [2, 3], which focused on the atomic pseudopotential; the crystal pseudopotential is written as a superposition of the atomic ones. Those expressions adopted a model approach, i.e., a model functional form was proposed that includes several parameters which are then evaluated in order to reproduce some experimental properties. In particular the Heine–Abarenkov model pseudopotential [2] is given by

$$v_{\mathrm{ps}}^{\mathrm{HA}}(r) = \begin{cases} -Z_v/r & r > R_M \\ -\sum_l A_l(E)\mathcal{P}_l & r < R_M \end{cases}$$

where R_M is a model radius, to be taken as greater than or equal to the core radius, $A_l(E)$ are energy-dependent constants, and $\mathcal{P}_l$ is a projector operator, which picks out the lth angular momentum component of the wavefunction. Shaw's optimized model potential [3] allows an l-dependent model radius $R_M(l)$ to be chosen so as to make the pseudopotential continuous at $R_M(l)$.

The main idea behind these simpler expressions is that the form of the pseudopotential inside the core does not matter, as long as it reproduces the scattering properties of the true potential outside the core. Therefore, it is expected that by making a proper choice of the parameters, these scattering properties can be conveniently recovered. In fact, the usual practice was to fit the constants $A_l(E)$ so as to reproduce the experimental spectral properties of the free ion in several electronic configurations and to use the pseudopotential obtained to compute, for instance, the band structure of the crystal. However, changes of the parameters were sometimes needed in order to obtain good agreement with experiment, giving rise to the problem of the *transferability* of the pseudopotential from one environment to another. When the fitting was performed on metals, the experimental Fermi surface was often used as an input. However, due to crystal symmetry, the pseudopotential enters for wave vectors corresponding to the reciprocal lattice only. Another piece of information useful for fitting was the phonon spectrum of the crystalline metal; this has the advantage of involving the pseudopotential for all wave vectors, not only those imposed by the crystal symmetry. This illustrates that dynamic properties of the systems are useful in order to produce a good pseudopotential, or to decide whether a given pseudopotential qualifies as good enough.

More recently, the construction of pseudopotentials has shifted again from modelling towards *ab initio* construction. Much of the interest in the subject has emerged from the development of *ab initio* methods, which rely on density functional theory, to perform molecular dynamics simulations. In principle, these methods can provide a lot of information (electronic, static, and dynamic properties) which enable a comparison with experiment and therefore represent an important test of the quality of the pseudopotential.

In this contribution we focus on the dynamic properties of liquid metals, and their relation to the pseudopotentials. In section 2 we briefly describe some dynamic properties of liquid systems, as well as some available methods of calculation, in particular molecular dynamics simulations. In advance, the evaluation of the total energy of the system is required, and in section 3 we will discuss two methods for obtaining it (specifically for the case of simple liquid metals and alloys), namely, linear response theory (perturbation theory) and density functional theory. Both approaches make use of pseudopotentials in order to make the computations feasible, and in section 4 we will describe several methods for constructing convenient pseudopotentials which can describe the interactions between ions and valence electrons. Finally, we will end up with some examples of the application of the present formalism to study some dynamic properties of several pure metals (Li, Mg, Al) near their respective triple points, and of one phase-separating binary alloy, LiNa, at a temperature and concentration close to its upper consolute point, near the demixing region.

2. Dynamic properties of liquids

The basic magnitudes for describing the dynamic properties of a system are the time correlation functions of several dynamic variables of the system. We will first define some dynamical variables, and their correlation functions will be considered later. We will also briefly discuss the behaviour of these correlation functions in different dynamic regimes and its relation to experimental measurements.

2.1. Basic dynamic variables

The self-number density of particle j is defined as

$$\rho_{s;j}(\vec{r}, t) = \delta(\vec{r} - \vec{R}_j(t)) \tag{1}$$

where $\vec{R}_j(t)$ denotes the position of particle j at time t. Its associated space Fourier transform (FT) will be denoted as $\rho_{s;j}(\vec{k}, t)$

The (collective) number density of particles of a given type is defined as the sum of all the self-number densities of particles of that type. We will assume throughout that we are dealing with one-component systems, although the generalization to multicomponent mixtures is straightforward. Thus, the number density for a one-component system is defined as

$$\rho(\vec{r}, t) = \sum_j \delta(\vec{r} - \vec{R}_j(t)) \tag{2}$$

and its space FT will be denoted as $\rho(\vec{k}, t)$.

The current density of particles of a given type is also an important dynamic variable; it is defined as

$$\vec{j}(\vec{r}, t) = \sum_j \vec{V}_j(t)\delta(\vec{r} - \vec{R}_j(t)) \tag{3}$$

where $\vec{V}_j(t)$ is the velocity of particle j at time t. In fact the particle velocity itself is also an important dynamic variable which will be considered later on. The corresponding space FT, $\vec{j}(\vec{k}, t)$, is usually decomposed into a longitudinal (parallel to $\vec{k}$) component $\vec{j}_l(\vec{k}, t)$ and a transverse (perpendicular to $\vec{k}$) component $\vec{j}_t(\vec{k}, t)$, with $\vec{j}(\vec{k}, t) = \vec{j}_l(k, t) + \vec{j}_t(k, t)$.

There are also other dynamic variables related to the dynamic properties of a system, like the stress tensor and the energy current density, that will not be discussed here. Instead, we refer the reader to the many books and reviews on the subject; see, for instance, reference [4].

2.2. Correlation functions

The time correlation functions for dynamic variables are the basic magnitudes used to describe the dynamic properties. Particularly important are the time autocorrelation functions of the dynamic variables considered in the previous subsection.

The time autocorrelation function associated with $\rho_{s;j}(\vec{k}, t)$ defines the self-intermediate-scattering function

$$F_s(k, t) = \left\langle \rho_{s;j}(\vec{k}, t + t_0)\rho_{s;j}(-\vec{k}, t_0) \right\rangle \tag{4}$$

where, assuming that we are dealing with homogeneous and isotropic bulk system, the average $\langle \cdots \rangle$ is carried out over time origins t_0, particles of the same type (i.e. all the particles) j, and directions of the wave vector $\vec{k}$. The Fourier transform to real space of $F_s(k, t)$ is the van Hove self-function $G_s(r, t)$, which is related to the probability that a given particle has moved a distance r in a time interval t. On the other hand, the Fourier transform of $F_s(k, t)$ into the frequency domain is the self-dynamic structure factor $S_s(k, \omega)$, which is directly related to the incoherent intensity obtained in an inelastic neutron scattering experiment; i.e. it is an experimentally accessible property.

The intermediate-scattering function is defined as

$$F(k, t) = \frac{1}{N} \left\langle \rho(\vec{k}, t + t_0)\rho(-\vec{k}, t_0) \right\rangle \tag{5}$$

where N is the number of particles, and the average is now over time origins t_0 and over directions of $\vec{k}$. For multicomponent mixtures the factor $1/N$ is replaced by $1/\sqrt{N_\alpha N_\beta}$ in the definition of $F_{\alpha\beta}(k, t)$, where α and β run from 1 to the number of different species and N_α is the number of particles of species α. The Fourier transform to real space of $F(k, t)$ is the van Hove function $G(r, t)$, which is related to the probability that if one particle is at the origin at a certain time, then any particle (the same or a different one) will be at a distance r from

the origin after a time interval t. The FT to the frequency domain of $F(k,t)$ is the dynamic structure factor $S(k,\omega)$, which is also experimentally accessible, since it is directly related to the coherent intensity obtained in an inelastic neutron or x-ray scattering experiment.

The longitudinal and transverse current correlation functions are defined as

$$C_l(k,t) = \frac{1}{N}\left\langle \vec{j}_l(\vec{k}, t+t_0)\cdot\vec{j}_l(-\vec{k},t_0)\right\rangle \tag{6}$$

$$C_t(k,t) = \frac{1}{2N}\left\langle \vec{j}_t(\vec{k}, t+t_0)\cdot\vec{j}_t(-\vec{k},t_0)\right\rangle. \tag{7}$$

Due to its definition, the longitudinal current correlation function is directly related to the intermediate-scattering function, or, in the frequency domain, to the dynamic structure factor:

$$C_l(k,t) = -\frac{1}{k^2}\frac{\mathrm{d}^2F(k,t)}{\mathrm{d}t^2} \qquad C_l(k,\omega) = \frac{\omega^2}{k^2}S(k,\omega) \tag{8}$$

and can therefore be measured experimentally. The situation is however different for the transverse current correlation function, which is not accessible to experiment.

Two further correlation functions, not directly accessible to experiment, are the velocity autocorrelation function, $Z(t)$, and the closely related mean square displacement, $\delta r^2(t)$, of a given particle in the system:

$$Z(t) = \left\langle \vec{V}_j(t+t_0)\cdot\vec{V}_j(t_0)\right\rangle \tag{9a}$$

$$\delta r^2(t) = \left\langle \left|\vec{R}_j(t+t_0) - \vec{R}_j(t_0)\right|^2\right\rangle = 2\int_0^t \mathrm{d}\tau\ (t-\tau)Z(\tau) \tag{9b}$$

where, for a homogeneous bulk system, the average is over time origins and over particles of the same type. Both functions are related to the diffusion coefficient, D, which is a measurable quantity, either as the time integral of $Z(t)$ or as the slope of $\delta r^2(t)$ (divided by 6) at long times.

2.3. Dynamic regimes

Taking into account the relationship between the wave vector and the mean interparticle distance d and between the frequency and the mean collision time τ, three dynamic regimes can be considered.

(i) The hydrodynamic regime, characterized by $kd \ll 1$ and $\omega\tau \ll 1$. Now the wavelength comprises many particles; the typical times involve many collisions and therefore the situation can be described as the evolution of a continuum fluid, to which the hydrodynamic equations can be applied, leading to the following behaviour of the previous correlation functions. The self-dynamic structure factor, $S_s(k,\omega)$, is a Lorentzian centred at $\omega = 0$, with height $1/(\pi Dk^2)$, and its halfwidth at half-maximum is Dk^2. The dynamic structure factor $S(k,\omega)$ is approximately the sum of three Lorentzians, one centred at $\omega = 0$ and two centred at $\omega = \pm c_s k$, with c_s being the adiabatic sound velocity. These side peaks represent longitudinal collective excitations in the liquid, and are interpreted as sound propagation, being similar in character to phonons in solid systems. $C_l(k,\omega)$ is just proportional to the dynamic structure factor multiplied by ω^2, and therefore it has side peaks representing longitudinal collective excitations. On the other hand $C_t(k,\omega)$ is also a monotonically decaying Lorentzian centred at $\omega = 0$, whose height and width are related to the shear viscosity of the liquid. It does not have any side peaks and therefore in this regime no transverse collective excitations are supported, contrary to the behaviour in solid systems.

(ii) The free-particle regime characterized by $kd \gg 1$ and $\omega\tau \gg 1$. Now, the wavelength is much shorter than the mean interparticle distance and the typical time is much smaller than the mean collision time. Therefore each particle practically does not feel the presence of the others and the behaviour of the correlation functions is the following. The self-dynamic structure factor and the dynamic structure factor coincide and are described by a monotonically decaying Gaussian centred at $\omega = 0$, whose height and width are related to the thermal velocity, $v_{\text{th}} = \sqrt{k_B T/m}$, where k_B is the Boltzmann constant and T is the temperature. No side peaks appear in $S(k, \omega)$ and consequently no longitudinal collective excitations appear in this regime. $C_l(k, \omega)$, on the other hand, is again proportional to ω^2 times a Gaussian, and this function does have side peaks, which have no physical meaning. The transverse $C_t(k, \omega)$ is again a Gaussian showing no transverse collective excitations.

(iii) The kinetic regime, where $kd \approx 1$ and $\omega\tau \approx 1$. Now there is no simplifying assumption and the correlation functions must be either calculated or measured (when possible). For example, inelastic neutron scattering (INS) provides a linear combination of $S_s(k, \omega)$ and $S(k, \omega)$ through the incoherent and coherent intensities whereas inelastic x-ray scattering (IXS) is purely coherent and therefore provides direct information on the dynamic structure factor $S(k, \omega)$. For the calculation of the correlation functions, two approaches can be followed, namely molecular dynamics (MD) simulations and theoretical methods. Nevertheless, the general shape of the correlation functions is as follows. $S_s(k, \omega)$ is always a monotonically decaying function of ω, whose main features are embodied in its height and width [5,6]. The dynamic structure factor may exhibit side peaks representing longitudinal collective modes. The side peaks appear for a range of k-values depending on the nature of the system. For instance, in liquid Ar the maximum k is around 0.07 k_p [7,8] (k_p is the main peak position of the static structure factor, $S(k)$) which means that the minimum wavelength of the supported collective longitudinal excitations is around 12 times the mean interparticle distance. On the other hand, for liquid Rb the maximum k is around 0.7 k_p [7, 9], i.e., the minimum wavelength is around 1.2 times the mean interparticle distance. The longitudinal current, $C_l(k, \omega)$, always shows side peaks which do not always (as in the free-particle regime) represent real longitudinal collective modes. Finally, $C_t(k, \omega)$ may or may not exhibit side peaks representing transverse collective excitations. This is not a measurable function and only MD results are known. Usually the transverse excitations appear only in a limited region of wave vectors depending on the nature of the liquid. In liquid Ar the minimum k that supports transverse collective modes is around 0.13 k_p (note that in this case there is no range of k-values where longitudinal and transverse excitations coexist), whereas in liquid Rb this minimum k is about 0.065 k_p (i.e., there is a large k-region where both transverse and longitudinal waves are supported, in closer analogy to a solid system) [8].

2.4. Calculation of dynamic properties; MD simulations

All dynamic properties depend on the time evolution of the positions and velocities of the particles; therefore, if these were known as a function of time, the dynamic properties could be evaluated. MD simulations provide exactly this information, and therefore they are extremely useful for the study of time-dependent properties. They even give information on magnitudes which are not accessible to experiment. The way MD simulations work is extremely simple, in principle. Given a set of N particles, and an initial configuration (positions and velocities) $\{\vec{R}_1, \vec{V}_1; \vec{R}_2, \vec{V}_2; \ldots; \vec{R}_N, \vec{V}_N\}$, the total potential energy is calculated, $E_{\text{pot}}(\vec{R}_1, \vec{R}_2, \ldots, \vec{R}_N)$, and therefrom the force on each atom is obtained, $\vec{F}_j = -\vec{\nabla}_j E_{\text{pot}}$. Then, Newton's equations are numerically solved (they are second-order differential equations) to find the positions and

velocities of the particles after a time interval, Δt. For this new configuration the potential energy and the forces are again evaluated and Newton's equations solved to obtain the following configuration after another time interval Δt. This procedure is iterated for a given number of configurations, $N_{\rm it}$, leading finally to a set of values of positions and velocities of the particles of the system at times $t_n = n\,\Delta t$, with $n = 0, 1, \ldots, N_{\rm it}$, from which the dynamic properties are computed. When dealing with bulk systems, and in order to eliminate surface effects, the particles are enclosed in a box (we assume it to be cubic, which is very usual) of volume $V = L^3$ so that the correct experimental density is obtained, and the box is repeated periodically, leading to the so-called periodic boundary conditions. Periodic boundary conditions have two important consequences on the structural quantities obtained in the simulation. First, the r-dependent quantities are meaningful for distances smaller than $L/2$. Second, for k-dependent properties, only those wave vectors compatible with the periodicity are allowed, i.e. $\vec{k}$ must be in the reciprocal lattice associated with the periodic boundary conditions imposed. In particular the minimum k-value allowed in the simulation is $2\pi/L$ which makes it quite difficult to reach the hydrodynamic regime. Finally, notice that the essential input to MD simulations is the potential energy of the system as a function of its configuration. This potential energy is computed within the Born–Oppenheimer approximation, in which the electrons are always in the ground state, the ionic positions act as parameters in the electronic Hamiltonian, and the electronic ground-state energy plays the role of an extra potential energy for the ions, to be added to their direct interaction. Now, depending on how this electronic ground-state energy, and therefore $E_{\rm pot}$, is computed, the MD simulations can be classified into classical simulations (CMD) and *ab initio* simulations (AIMD). In CMD the potential energy is usually written in terms of n-body potentials, up to $n = 2$ (i.e. pair potentials) in most cases:

$$E_{\rm pot}(\{\vec{R}_\alpha\}) = \varphi^{(0)} + \sum_j \varphi^{(1)}(\vec{R}_i) + \frac{1}{2}\sum_{i\neq j}\varphi^{(2)}(\vec{R}_i, \vec{R}_j) \tag{10}$$

although sometimes further terms are also included. In the case of simple liquid metals both the ground-state energy and electronic density can be obtained by using linear response theory (LRT), i.e. pseudopotential perturbation theory, up to first order for the electron density, up to second order for the energy, taking as reference system a homogeneous electron gas (jellium). The result for the potential energy is of the form exhibited in equation (10) but without one-body terms. On the other hand, in AIMD the $E_{\rm pot}$ depends parametrically on all the positions of the ions, and is obtained, along with the ground-state electron density, by using density functional theory (DFT), considering however only valence electrons and pseudopotentials to describe their interactions with ions.

3. Potential energy calculation

We have seen that the potential energy is the key ingredient enabling the calculation of the dynamic properties of the system. Although, in principle, an electronic theory such as DFT can deal with core and valence electrons, in practice an explicit treatment of the core electrons would be much too demanding; therefore usually only the valence electrons are explicitly considered using pseudopotentials, while the inner-core electrons are joined to the nucleus to form an ion. On the other hand, a perturbative theory like LRT requires that the perturbation be weak and, given that the true potential is far from being weak, the use of pseudopotentials becomes absolutely necessary.

In the following we will assume that the interaction between ions and valence electrons can be described in terms of a local energy-independent pseudopotential. Although it is a simplification, the following applications will show its ability to provide a proper description

of several static and dynamic properties of different systems. Moreover, the equations to be solved become simpler; however, we will indicate where the equations should be modified in the case of non-local pseudopotentials (energy dependence will not be considered at all).

The total potential energy of a system of N ions of valence Z, enclosed in a volume V, which interact with $N_e = NZ$ valence electrons through a local pseudopotential $v(r)$, is written, within the Born–Oppenheimer approximation, as the sum of the direct ion–ion interaction energy, which we assume Coulombic, and the ground-state energy of the electronic system subject to the external potential created by the ions, $V_{\rm ext}(\vec{r}, \{\vec{R}_l\}) = \sum_{i=1}^{N} v(|\vec{r} - \vec{R}_i|)$:

$$E(\{\vec{R}_l\}) = \sum_{i<j} \frac{Z^2}{|\vec{R}_i - \vec{R}_j|} + E_g[\rho_g(\vec{r}), V_{\rm ext}(\vec{r}, \{\vec{R}_l\})] \tag{11}$$

where $\rho_g(\vec{r})$ is the ground-state electron density.

3.1. Linear response theory (for metals)

According to LRT, the ground-state electron density is given, in reciprocal space, by

$$\rho_g^{\rm LRT}(\vec{q}) = \left(\sum_l e^{i\vec{q}\cdot\vec{R}_l}\right) n^{\rm LRT}(q) \equiv F(\vec{q}) n^{\rm LRT}(q) \tag{12}$$

$$n^{\rm LRT}(q) = \chi(q, \rho_0) v(q) \tag{13}$$

where $\chi(q, \rho_0)$ is the response function of a uniform electron gas of density $\rho_0 = N_e/V$. These equations imply that the ground-state electron density is a superposition of spherically symmetric pseudoatomic densities around each ion, i.e.,

$$\rho_g^{\rm LRT}(\vec{r}) = \sum_l n^{\rm LRT}(|\vec{r} - \vec{R}_l|). \tag{14}$$

The ground-state energy is also given as

$$E_g^{\rm LRT} = E_v[\rho_0] + \sum_{i<j} \phi_{\rm ind}(R_{ij}; \rho_0) \tag{15}$$

where $\phi_{\rm ind}(q; \rho_0) = \chi(q, \rho_0) v^2(q)$ and E_v is a structure-independent term. Therefore, the total potential energy of equation (11) can be written, within LRT, as a sum of a structure-independent term and a sum over pairs of an effective density-dependent pair potential $\phi_{\rm eff}(R; \rho_0) = Z^2/R + \phi_{\rm ind}(R; \rho_0)$. This leads to a picture of the metal as a collection of pseudoatoms, made up by the ions and the associated electronic screening clouds $n(r)$, interacting through these state-dependent pair potentials.

For non-local pseudopotentials the final picture is the same, but the equations relating the pseudopotential to the screening density, on one hand, and with the ground-state energy, on the other, are more involved [10]. Moreover, an important difference is that for local pseudopotentials there is a one-to-one correspondence between the screening electronic cloud, $n(q)$, and the induced interaction $\phi_{\rm ind}(q)$—namely $\phi_{\rm ind}(q) = n(q)v(q)$; therefore, the electron density determines uniquely the potential energy. However, for non-local pseudopotentials this one-to-one correspondence is not guaranteed, so there could be different non-local pseudopotentials leading to the same electron density but with different potential energies [11].

3.2. Density functional theory

We will briefly comment on some aspects of DFT, and for further details the reader is referred to the original paper or some of the books and reviews on the subject [12]. When a system of N_e interacting electrons is placed in an external potential $V_{\rm ext}$ (usually created by the ions) then its

ground state can be obtained by finding the lowest eigenvalue and corresponding eigenvector of the Hamiltonian. By solving the associated time-independent Schrödinger equation, the ground-state energy E_g, the ground-state wavefunction $\psi_g(\vec{r}_1, s_1; \vec{r}_2, s_2; \ldots; \vec{r}_{N_e}, s_{N_e})$, and the ground-state electron density, $\rho_g(\vec{r})$, can be obtained.

In this context, some important points of DFT are worth mentioning. First, the ground-state density determines uniquely the external potential and therefore the Hamiltonian and the ground-state wavefunction ψ_g. Second, it also determines the ground-state expectation value of any observable, which in the case of the Hamiltonian is the ground-state energy, E_g. So finally the ground-state density $\rho_g(\vec{r})$ determines the ground-state energy E_g. Mathematically, this is expressed by saying that the ground-state energy is a functional of the ground-state density, $E_g = E[\rho_g(\vec{r})]$. The third important point, essential for calculations, is that this functional has the following variational property: for a fixed external potential the functional evaluated for any density $\rho(r)$ takes a value which is greater than or equal to E_g; in other words, the ground-state density $\rho_g(\vec{r})$ minimizes the functional, and this minimum value is precisely E_g. The fourth point is that if the functional is written as the sum of the energy of interaction with the external potential plus the rest of the energy, then this second part is a *universal* functional, which means that it does not depend on the external potential, i.e. it is the same for atoms, molecules, liquids, and so on.

Summarizing, DFT states that in order to calculate the electronic ground-state energy and density, one does not need the complicated antisymmetric ground-state wavefunction, which depends on $3N_e$ spatial variables and N_e spin variables, but instead both of them can be obtained by minimizing an energy functional, which can be written as

$$E[\rho(\vec{r})] = T_s[\rho(\vec{r})] + E_{\text{ext}}[\rho(\vec{r})] + E_H[\rho(\vec{r})] + E_{\text{xc}}[\rho(\vec{r})]. \tag{16}$$

The terms represent, respectively, the electronic kinetic energy, T_s, of a non-interacting system of density $\rho(\vec{r})$, the energy of interaction with the external potential created by the ions,

$$E_{\text{ext}} = \int \mathrm{d}\vec{r}\ \rho(\vec{r}) V_{\text{ext}}(\vec{r}) \tag{17}$$

and the classical electrostatic energy (Hartree term),

$$E_H = \frac{1}{2} \int \int \mathrm{d}\vec{r}\ \mathrm{d}\vec{s}\ \frac{\rho(\vec{r})\rho(\vec{s})}{|\vec{r} - \vec{s}|} \tag{18}$$

and also the exchange–correlation energy, E_{xc}, which is just the rest of the energy, and includes part of the true kinetic energy and other effects due to indistinguishability (exchange) and correlation. Below we consider explicitly the two complicated terms of the functional, namely, the exchange–correlation functional and the kinetic energy functional.

The exact expression for E_{xc} is unknown, but several useful approximations have been proposed. A widely used expression is the so-called local density approximation (LDA)

$$E_{\text{xc}}^{\text{LDA}}[\rho(\vec{r})] = \int \mathrm{d}\vec{r}\ \rho(\vec{r}) \epsilon_{\text{xc}}^{(0)}(\rho(\vec{r})) \tag{19}$$

where $\epsilon_{\text{xc}}^{(0)}(n)$ is the exchange–correlation energy density of a uniform electron gas of density n, which is known through simulations [13] and further fittings [14, 15]. Other more elaborate approximations have been proposed [16–18], but here we will only consider those applications where the LDA expression is used.

Contrary to the case for E_{xc}, it is possible to calculate exactly the kinetic energy functional T_s. This is accomplished through the introduction of single-particle orbitals [19], in the so-called Kohn–Sham representation of density functional theory (KS-DFT). The use of orbitals somewhat complicates the simplicity of the original representation where just the electron

density appears, i.e., the orbital-free density functional theory (OF-DFT). If one sticks to OF-DFT, the exact functional form of $T_s[\rho(\vec{r})]$ is unknown, and therefore approximate expressions must be used. We consider below the two approaches (KS and OF) separately.

3.2.1. Exact calculation of T_s: KS-DFT. It was shown by Kohn and Sham [19] that minimizing $E[\rho(\vec{r})]$ while keeping N_e fixed, is equivalent to diagonalizing a one-particle Hamiltonian

$$H_{\mathrm{KS}} = -\frac{1}{2}\vec{\nabla}^2 + V_{\mathrm{ext}} + V_H[\rho(\vec{r})] + V_{\mathrm{xc}}[\rho(\vec{r})] \tag{20}$$

where $V_H(r) = \int \mathrm{d}\vec{s}\ \rho(\vec{s})/|\vec{r} - \vec{s}|$, and V_{xc} are the functional derivatives of E_H and E_{xc} respectively. The diagonalization leads to the eigenvalues ϵ_i and the orbitals $\varphi_i(\vec{r})$, from which the ground state is constructed:

$$\rho_g(\vec{r}) = \sum_{\mathrm{occ}} |\varphi_i(\vec{r})|^2 \tag{21}$$

where the sum runs over occupied states, which are the lowest-lying ones, up to the Fermi energy. Finally, the kinetic energy that we were looking for is

$$T_s = \sum_{\mathrm{occ}} \int \mathrm{d}\vec{r}\ \varphi_i^*(\vec{r})\left(-\frac{1}{2}\vec{\nabla}^2\right)\varphi_i(\vec{r}). \tag{22}$$

It is important to notice that the eigenstates, and therefore the electronic density, depend on the Hamiltonian, and in particular on the Hartree and exchange–correlation potentials, which themselves depend on the density. So we are faced with a situation where a self-consistent scheme is required. We also note that when a non-local pseudopotential between ions and valence electrons is used, expression (17) for the external energy is not valid any more, and has to be replaced with one where the orbitals appear explicitly.

3.2.2. Approximate calculation of T_s: OF-DFT. As already stated, the exact expression for T_s in terms of $\rho(\vec{r})$ is unknown. However, it is considered [20] that the von Weizsäcker term

$$T_W[\rho(\vec{r})] = \frac{1}{8}\int \mathrm{d}\vec{r}\ |\nabla\rho(\vec{r})|^2/\rho(\vec{r}) \tag{23}$$

is essential for a good description of the kinetic energy. It is the leading term for rapidly varying densities and, furthermore, it is exact for one- and two-electron systems, and for systems composed of one- or two-electron separated subsystems. Usually further terms are added in order to reproduce correctly some exactly known limits. In the uniform-density limit, the exact kinetic energy is given by the Thomas–Fermi functional:

$$T_{\mathrm{TF}}[\rho(\vec{r})] = \frac{3}{10}\int \mathrm{d}\vec{r}\ \rho(\vec{r})k_F(\vec{r})^2 \tag{24}$$

where $k_F(\vec{r}) = (3\pi^2)^{1/3}\rho(\vec{r})^{1/3}$ is the local Fermi wave vector. In the limit of almost uniform density, LRT is correct, with the response function corresponding to a non-interacting uniform electron gas, i.e. the Lindhard function [21], $\chi_L(q, \rho_0)$.

Recently, there has been renewed interest in the development of accurate kinetic energy functionals, partly because of the advantages of the orbital-free *ab initio* simulations. Among several proposals [22–26], we mention the expression proposed by García-González *et al* [27] which has been used in this work, although in a simplified version which is amenable to

rapid evaluation through the use of fast Fourier transform (FFT) routines. We have used for $T_s = T_W + T_\beta$

$$T_\beta = \frac{3}{10}\int \mathrm{d}\vec{r}\ \rho(\vec{r})^{5/3-2\beta}\tilde{k}(\vec{r})^2 \tag{25a}$$

$$\tilde{k}(\vec{r}) = (2k_F^0)^3 \int \mathrm{d}\vec{s}\ k(\vec{s})w_\beta(2k_F^0|\vec{r}-\vec{s}|) \tag{25b}$$

where $k(\vec{r}) = (3\pi^2)^{1/3}\rho(\vec{r})^\beta$, k_F^0 is the Fermi wave vector corresponding to the mean electron density ρ_0, and $w_\beta(x)$ is a weight function, determined by requiring the correct recovery of both the LRT limit and the uniform-density limit. Note that $\tilde{k}(\vec{r})$ is obtained as a convolution, which can be performed rapidly with the usual FFT techniques.

A detailed account of this functional will be published elsewhere [28], but we just mention here that it is positive definite, and for a range of values of β, namely $0.5 < \beta < 0.566$, fulfils other useful mathematical requirements related to the finite character of the functional derivative for small densities. In the applications we have used a value of $\beta = 0.51$.

3.3. Molecular dynamics for liquid metals and alloys

Three different classes of MD simulations for liquid metals and alloys will be considered here. First, CMD calculations with interatomic pair potentials obtained from LRT; they will be referred to as LRT-CMD simulations. Second AIMD calculations where the KS representation of DFT is used and they will be referred to as KS-AIMD simulations. Thirdly, AIMD calculations where the OF-DFT is used, which will be called OF-AIMD simulations.

Most AIMD calculations performed to date have been KS-AIMD simulations. In this type of simulations N ions are enclosed in a box of volume V with periodic boundary conditions, the interaction between ions and valence electrons is described by means of non-local pseudopotentials, the electronic ground-state energy is computed using KS-DFT with an approximate E_{xc} (usually LDA), the orbitals are expanded in plane waves compatible with the periodic boundary conditions, and either H_{KS} is diagonalized until self-consistency is achieved, or $E[\rho(\vec{r})]$ is minimized imposing orthonormalization constraints on the orbitals, and finally the forces are obtained from the gradients of the potential energy in order to move the atoms. There is a third possibility where the ground state is not found exactly for each configuration (only for the initial one), but instead it is updated via a time evolution governed by a coupled ion–electron Lagrangian which also includes dynamic orbital orthonormalization constraints; this is the Car–Parrinello approach [29], which, however, is not well suited for the study of those systems where no gap exists between occupied and unoccupied electron states [30], as is the case for metals.

Starting with the pioneering work of Madden and co-workers [31] several OF-AIMD simulations have recently been performed for metallic systems. Now, N ions are enclosed in a box of volume V with periodic boundary conditions, local pseudopotentials are used (in fact *must be used*) to describe the interaction between ions and valence electrons, the electronic ground-state energy is computed using OF-DFT with approximate expressions for T_s and E_{xc} (usually LDA), the electron density (or sometimes its square root) is expanded in plane waves compatible with the periodic boundary conditions, and $E[\rho(\vec{r})]$ is minimized imposing the normalization constraint on the density (which must integrate to the number of electrons); finally the forces are obtained from the gradients of the potential energy in order to move the atoms.

In both KS-AIMD and OF-AIMD simulations, the minimization of the functional is performed with respect to the coefficients of the respective expansions in plane waves. The

number of coefficients (which are the variables for minimizing the energy) is very large, especially in the case of KS-AIMD. For instance, in an early study of liquid Mg [32] with 90 ions, which means 180 valence electrons and 90 doubly occupied orbitals, and truncating the expansion in plane waves at wave vectors corresponding to a kinetic energy of 12 Ryd (this is the so-called cut-off energy), the number of complex coefficients representing the 90 orbitals is around half a million. Moreover, imposing the orthonormalization constraints requires a lot of computer time and scales very badly, $O(N^3)$, with the number of ions in the simulation box. The situation with KS-AIMD can be briefly summarized by saying that this method is extremely burdensome computationally; consequently most studies have dealt with static structural properties and diffusion coefficients only. To our knowledge, there has been just one study, on liquid Li near melting, which also evaluated collective dynamical magnitudes [33]. On the other hand, in OF-AIMD simulations the number of coefficients is much smaller, because there is only one function (the electronic density) to be expanded, and moreover the normalization constraint is almost trivial. Therefore, much less computer time is required and the scaling with the number of atoms is also much better, $O(N \log N)$. Summarizing, although OF-AIMD calculations are still computationally burdensome, the calculation of dynamical magnitudes is feasible; in fact, there have already been a number of them [31, 34], and later on we will present several more. However, good approximate kinetic energy functionals are still required as well as good local pseudopotentials. We have touched briefly upon the first issue previously; we now focus on the second one.

4. Pseudopotential construction

We consider two basic methods for pseudopotential construction.

The first one is modelling, i.e. a model functional form is assumed with several parameters to be fitted so as to reproduce some property, previously determined by either experiment or from all-electron *ab initio* calculations. Among non-local models, we have already mentioned the Heine–Abarenkov model potentials whereas in the case of local models we may cite the well known empty-core pseudopotential (with one adjustable parameter) [35] or the recently proposed evanescent-core pseudopotential (with two parameters) [36].

The second route to pseudopotential construction is the *ab initio* method, whose basic idea is as follows. First, consider a 'reference state' for the atom that we are studying, which is simple enough that one can compute accurately, via Kohn–Sham density functional theory (KS-DFT), its electronic properties. Second, since the interest is in the valence electrons, we eliminate all of those effects on the valence properties which are due to the presence of core electrons; this step is called 'pseudizing' the valence properties. Third, consider what the pseudopotential is going to be used for, and how it is going to be used. Usually it will be used for the calculation of the ground-state energy of a complex system, probably composed of many atoms. This calculation can be carried out using several different theoretical approaches, for instance, KS-DFT, LRT, or OF-DFT. So the third step selects the appropriate theoretical approach to use in the study of the complex system. Finally, replace our atom in the 'reference state' by an effective potential, and apply the selected theoretical approach to calculate those valence properties considered in the second step. The pseudopotential is that effective potential which reproduces those valence properties.

Therefore, in the construction of the pseudopotential, three basic ingredients have to be specified: (i) the reference state, (ii) the valence properties on which we are going to focus, and (iii) the theoretical approach used in the study of the complex system. Below, we include two examples of this procedure that have been applied in the literature. The first is the 'standard' construction of non-local pseudopotentials for KS-AIMD [37, 38]. The second example is the

neutral-pseudoatom (NPA) method for constructing local pseudopotentials to be used within LRT in order to obtain effective interatomic pair potentials for simple metals [39]. Finally, we propose the application of the previous procedure to the construction of local pseudopotentials for OF-AIMD simulations.

4.1. Non-local pseudopotentials for KS-AIMD

The reference state is usually the free atom in its ground state. The valence properties considered are the energies and the wavefunctions corresponding to valence electrons or/and unoccupied states. These wavefunctions are pseudized, eliminating the oscillations near the nucleus which are due to the orthogonality with the core wavefunctions of the same angular momentum, l.

Finally, the theoretical approach to be used for the complex system is KS-DFT. Therefore, for each valence wavefunction a pseudopotential is found that, when used with KS-DFT, reproduces the same energies and pseudized wavefunctions as were constructed before. Now, the pseudopotential will be different for each l, i.e., it will depend on the angular momentum: a non-local pseudopotential.

4.2. NPA local pseudopotentials for simple metals

The environment of an atom in a metal is quite different from free space. Therefore it seems more appropiate to use a reference state which closely resembles this environment, while being simple enough that KS-DFT can still be applied to find the valence electronic properties.

Our reference state is the atom embedded in a uniform background (jellium) of density equal to the mean electron density of the complex system (the metal at some specified thermodynamic state), in which a spherical cavity has been made around the atom. This system still has spherical symmetry, like the free atom, and the main complication is that now the valence states are unbound, i.e., they are scattering states forming a continuum occupied up to the Fermi energy. The valence property considered is the 'displaced' valence electron density, $n(r)$—that is, the change in the electron density induced in the jellium due to the presence of the atom and the cavity. This is pseudized again by eliminating the core-orthogonality oscillations leading to $n_{\rm ps}(r)$.

Finally, the theoretical approach used for the complex system is LRT, and therefore we find an effective potential that when inserted into the same jellium along with the cavity will induce, within LRT, a displaced density equal to the pseudized one calculated previously, i.e., we use equation (13) to find $v_{\rm ps}(q) + v_{\rm cav}(q)$ from $n_{\rm ps}(q)$.

Now the pseudopotential is local and depends on the thermodynamic state, i.e., it is not transferable and must be calculated according to the mean electron density of the system.

4.3. Local pseudopotentials for OF-AIMD

For the same reasons as were previously explained, we use as the reference state the atom-in-jellium–cavity system and the valence property will also be the displaced valence electron density, which is pseudized as above.

The theoretical approach used for the complex system is OF-DFT. Therefore, we must find an effective potential that, when inserted into the jellium together with the cavity, will produce, within the OF-DFT theory, the same pseudized displaced density as was computed previously. Translated into formulae, it proceeds as follows. When the functional derivatives of the energy functional are performed, the Euler equation for our pseudopotential in the jellium–cavity

system is

$$\mu_s(r) + V_{\rm ext}(r) + V_H(r) + V_{\rm xc}(r) - \mu = 0 \tag{26}$$

where each term is the derivative of the corresponding term in equation (16), namely,

$$\mu_s(r) = \mu_W(r) + \mu_\beta(r) \tag{27}$$

corresponding to the von Weizsäcker term and the β-term in T_s respectively,

$$V_{\rm ext}(r) = v_{\rm ps}(r) + v_{\rm cav}(r) + v_{\rm jell}(r) \tag{28}$$

$$V_H(r) = \int {\rm d}\vec{s}\ \rho(s)/|\vec{r} - \vec{s}| \tag{29}$$

with $\rho(r) = \rho_0 + n(r)$, and $V_{\rm xc}(r)$ is the exchange–correlation potential. All the magnitudes depend on r only, due to the spherical symmetry. Inserting equations (27)–(29) into equation (26), we obtain an algebraic equation for the unknown $v_{\rm ps}(r)$ in terms of the known $\rho(r)$, whereas the constant μ is just an energy origin, which is fixed such that $v_{\rm ps}(r)$ decays to zero for large distances.

5. Results and discussion

5.1. Liquid Li

During the last decade, there has been a quite thorough study of the static and dynamic properties of liquid Li, by means of experimental, theoretical, and MD simulation methods, including LRT-CMD, KS-AIMD, and OF-AIMD. Among the dynamical studies, we mention the INS experiments of Verkerk and co-workers [40], the IXS experiments of Sinn *et al* [41], and those of Scopigno *et al* [42]. On the theoretical side, González *et al* [43] computed an empty-core pseudopotential [35] by fitting the results for the static structure factor to the neutron scattering ones of Ruppersberg and co-workers [44], and also constructed an *ab initio* NPA pseudopotential to be used within LRT. The interatomic pair potentials derived from the two pseudopotentials were used to compute by theoretical methods [43,45] and by LRT-CMD [46] methods the static and dynamic properties of liquid Li. Both pseudopotentials provided a good description of the static properties, but comparison with INS experiments [40] and IXS experiments [41] favoured the *ab initio* NPA pseudopotential over the model empty-core one. Regarding AIMD simulations, Kresse [33] performed the only KS-AIMD simulations (to our knowledge) where the dynamic structure factor was computed; Kresse used a non-local pseudopotential of the so-called ultrasoft type [47], which is designed especially for the elements of the first row of the periodic table and for transition metals. OF-AIMD simulations have been carried out by Anta and Madden, who have studied the static and dynamic [34] liquid structure; they used a kinetic energy functional which recovers the quadratic response function of the non-interacting homogeneous electron gas along with a local pseudopotential constructed by including in an approximate way the ionic structure of the liquid. The $S(k, \omega)$ obtained compared rather well with the IXS data [41] for all wave vectors considered. In contrast, the KS-AIMD results showed important disagreements in the small-k region, as the values of $S(k, \omega)$ obtained were about three hundred times larger than the experimental and the OF-AIMD ones.

Here, we present results of OF-AIMD simulations performed by using the simpler T_s-functional of equation (25*a*) combined with a pseudopotential constructed as indicated in section 4.3. We considered 205 particles enclosed in a cubic box of appropriate side such that the number density is $\rho = 0.044\,512\ \text{Å}^{-3}$, which is the experimental value at $T = 470$ K. The

cut-off energy in the plane-wave expansion was 15 Ryd, which amounts to 15 900 coefficients. The time step was 1 fs and the simulation lasted for 18 ps, after an initial equilibration of 5 ps.

Figure 1 shows the results obtained for the static structure factor, $S(k)$, along with the corresponding x-ray [48] and neutron [44] diffraction data. Our OF-AIMD results compare rather well with the experimental ones, being closer to the neutron data. At small k-values, our results are somewhat smaller than the neutron data, but still the agreement is rather good. The extrapolation of $S(k)$ to $k \to 0$, using a quadratic expression $S(k) = S(0) + ak^2$, leads to an isothermal compressibility $\kappa_T = S(0)/(\rho k_B T) \approx 0.8 \times 10^{-10}$ Pa^{-1}, to be compared with the experimental value [49] of 1.02×10^{-10} Pa^{-1}.

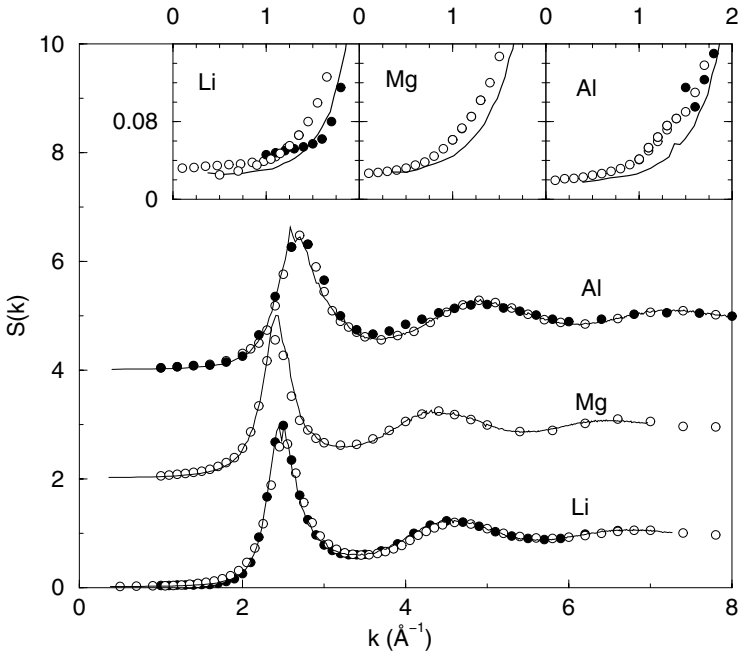

Figure 1. Static structure factors, $S(k)$, for the three metals studied. Note that the results for Mg have been shifted upward by two units and those for Al by four units. The insets show the low-k behaviour. Full lines: present OF-AIMD simulations. Open circles: x-ray diffraction data. Closed circles: neutron diffraction data.

The diffusion coefficient, derived from the slope of the mean square displacement, is $D = 0.66$ Å^2 ps^{-1} (these units will be used throughout) which compares favourably with the experimental value [50] of 0.64. The KS-AIMD simulations gave $D = 0.66$ whereas Anta and Madden's OF-AIMD simulations produced a lower value, namely $D = 0.55$. Finally, we mention that LRT-CMD simulations with the NPA pseudopotential lead to $D = 0.69$.

From the $F(k, t)$ obtained, the corresponding $S(k, \omega)$ are readily computed and in figure 2 we present the results for several k-values ($k/k_p = 0.29$, 0.5, 1, and 1.41). We also include the IXS data [41,42] as well as the OF-AIMD results of Anta and Madden. For small k-values, the experimental $S(k, \omega)$ exhibit well defined side peaks, which are typical of collective excitations, and they persist up to $k \approx 2/3k_p$. For $k = k_p$ a typical increase in the height and narrowing in frequency is found (the de Gennes narrowing) whereas for larger k a monotonic decay of $S(k, \omega)$ is obtained, leading to the free-particle behaviour. Both sets of IXS experimental data show good agreement, although the height of the peaks in Scopigno's data is a somewhat bigger. On the other hand, our OF-AIMD results show an overall qualitative agreement with

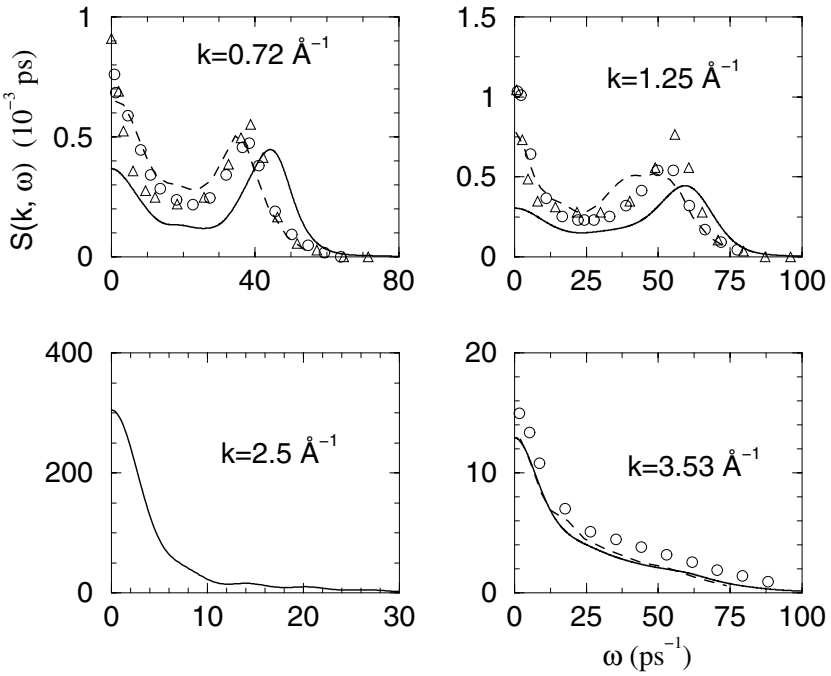

Figure 2. Dynamic structure factors, $S(k, \omega)$, for liquid Li. Full lines: present OF-AIMD simulations ($k = 0.76$, 1.25, 2.50, and 3.54 Å^{-1}). Dashed lines: Anta and Madden's OF-AIMD results ($k = 0.69$, 1.26, and 3.51 Å^{-1}). Open symbols: inelastic x-ray scattering data; circles: reference [41] (k-values shown on the graphs); triangles: reference [42] ($k = 0.70$ and 1.28 Å^{-1}).

experiment, although for small k-values our results underestimate the heights of the peaks, especially the central one. Comparison with the OF-AIMD results of Anta and Madden shows some discrepancies for small k-values which we ascribe to our use of a simpler T_s-functional; however, for larger k-values both OF-AIMD results almost coincide.

From the positions of the peaks of the dynamic structure factor, denoted by $\omega_m(k)$, or from those of the spectra of the longitudinal current correlation function $C_l(k, \omega)$, denoted as $\omega_l(k)$, a corresponding dispersion relation is obtained, which is shown in figure 3. The

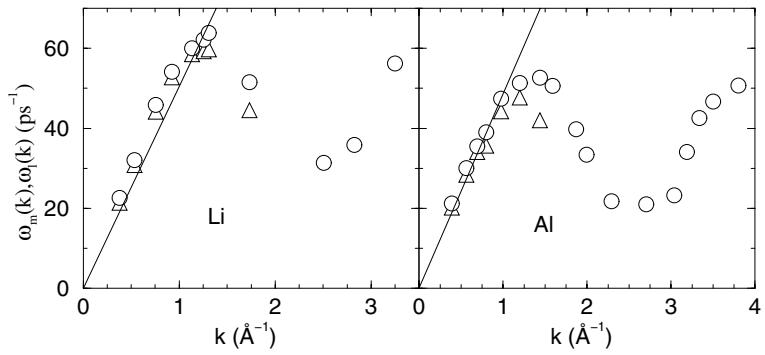

Figure 3. Dispersion relations of longitudinal collective modes for liquid Li and Al. Triangles: $\omega_m(k)$; circles: $\omega_l(k)$; lines: hydrodynamic dispersion (see the text).

isothermal sound velocity, obtained from the above-calculated isothermal compressibility, is 4900 m s^{-1}. By using the experimental ratio of specific heats, namely $\gamma = 1.06$ [49], this leads to an adiabatic sound velocity $c_s = 5050$ m s^{-1} which is somewhat higher than the experimental one obtained from the adiabatic compressibility [49] $c_s = 4550$ m s^{-1}. This is already apparent from figure 2 where the OF-AIMD side peak is somewhat shifted to the right of the experimental one (although there is also a certain k-mismatch). The hydrodynamic dispersion $\omega = c_s k$ (with the theoretical c_s) is shown in figure 3, where a positive dispersion is observed, i.e., the side peaks in $S(k, \omega)$ and $C_l(k, \omega)$ appear at frequencies higher than those corresponding to the hydrodynamic regime, which is only recovered for rather small values of k, not available in our simulations. Besides liquid Li, where the experimental positive dispersion shows a maximum at $k \approx 0.55$ Å^{-1} [41,42], this effect has also been experimentally observed in other liquid metals near melting, such as Na [51], Rb [52], Cs [53], and recently Al (see later).

5.2. Liquid Mg

In comparison with the case for the alkali metals, not much work, either theoretical or experimental, has yet been performed on the liquid alkaline-earth metals. Concerning the dynamical properties, we are only aware of LRT-CMD results (obtained with NPA potentials) of Alemany *et al* [54, 55], who report values of the diffusion coefficients (for Mg, $D = 0.665$ Å^2 ps^{-1}) and the intermediate- and self-intermediate-scattering functions. On the experimental side, no data on the dynamic structure factors or diffusion coefficients have yet been measured.

Restricting consideration to the static structural properties, several studies have already been performed. Among them, we mention the KS-AIMD simulations of de Wijs *et al* [32] and the OF-AIMD simulations of Anta *et al* [56], which show results for the static structure factor and for the electron–ion correlation functions. In the present OF-AIMD simulations of liquid Mg, at $T = 953$ K and $\rho = 0.038\,29$ Å^{-3}, we have used 205 particles, a time step of 1.5 fs, and a total averaging time of 25.5 ps after equilibration. The cut-off energy was 42.25 Ryd and the number of plane waves was around 85 000. Comparison with the KS-AIMD simulations (which used a cut-off energy of 12 Ryd and 500 000 coefficients) shows clearly the important memory savings achieved in OF-AIMD simulations, in spite of the larger cut-off required by local pseudopotentials.

The results obtained for $S(k)$, see figure 1, show good agreement with the experimental x-ray data, even in the small-k region. The diffusion coefficient obtained within the OF-AIMD simulations is $D = 0.53$ Å^2 ps^{-1}, which is somewhat smaller than the value from the LRT-CMD simulations. The dynamic structure factors obtained are shown in figure 4, for several k-values (at similar values of k/k_p to those shown for Li). The overall behaviour of $S(k, \omega)$ is very similar to that of liquid Li and other liquid metals, showing longitudinal collective modes for small wave vectors, a de Gennes narrowing at k_p, and a gradual transition to the free-particle regime for higher k. In figure 4 we have also included the $S(k, \omega)$ obtained from the LRT-CMD $F(k, t)$ data of Alemany *et al*. It is observed that whereas the side peaks obtained in LRT-CMD and OF-AIMD appear at the same frequency, the central peak is much higher in LRT-CMD simulations; this is due to a marked diffusive behaviour in the LRT-CMD $F(k, t)$ results, which is absent (or very weak) in the OF-AIMD results. Nevertheless, the two approaches lead to very similar dispersion relations. Moreover, since there are no experimental data for γ, it is difficult to envisage the possible existence of a positive dispersion in liquid Mg; however, the plot of $w_m(k)/k$ versus k exhibits a maximum (see figure 5) indicative of some positive dispersion.

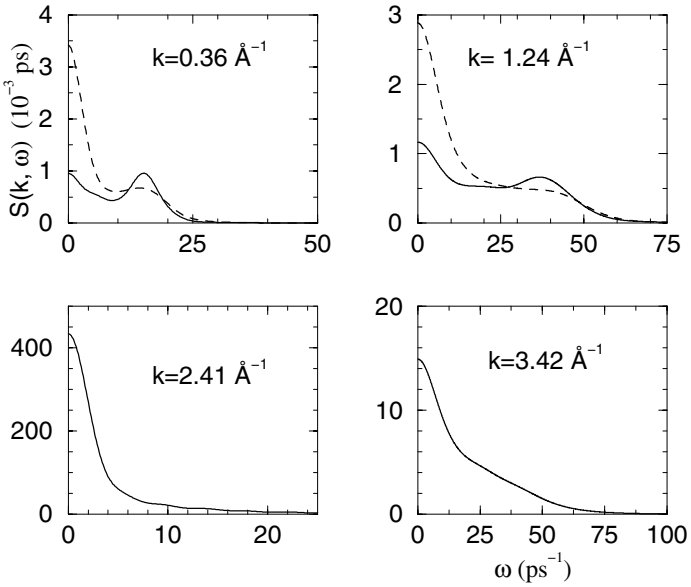

Figure 4. Dynamic structure factors of liquid Mg. Full lines: OF-AIMD results. Dashed lines: LRT-CMD results [55].

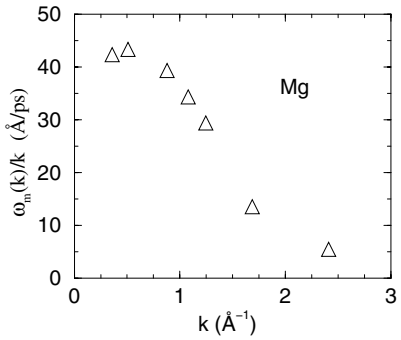

Figure 5. The phase velocity, $\omega_m(k)/k$, of the longitudinal collective modes for liquid Mg.

In summary, the OF-AIMD and the LRT-CMD simulations give rather similar results for the static structural magnitudes. However, the dynamic properties D and $S(k, \omega)$ as computed from the two approaches are rather different. Unfortunately, the lack of experimental data for the dynamical magnitudes prevents one from deciding which description is more accurate.

5.3. Liquid Al

Most studies of liquid Al have been performed using LRT-CMD with pair potentials derived from either local [57] or non-local [58] pseudopotentials. There has also been one KS-AIMD study [59] in which the static structure and the diffusion coefficient ($D = 0.60$ Å^2 ps^{-1}) were obtained, and an OF-AIMD simulation [56] which focused just on static structural properties, showing good agreement with the experimental structure factor of the liquid. Here we test the ability of the method (though with a different T_s-functional and a different pseudopotential)

to describe the dynamic structure of the system. We have considered a thermodynamic state with $T = 1000$ K and $\rho = 0.0524$ Å^{-3}, which is close to the triple point. We have used 205 particles, the time step was 1 fs, equilibration lasted for 10 ps, and averaging was performed for another 36 ps (36 000 configurations). The cut-off energy was 30 Ryd which amounts to about 85 000 plane-wave coefficients.

The OF-AIMD static structure factor obtained is shown in figure 1 together with the neutron [60] and x-ray [48] diffraction data. Comparison between the two sets of experimental data shows small differences in the region between 2 and 5 Å^{-1}, with the OF-AIMD results between the two sets, although closer to the x-ray ones. We note that LRT-CMD simulations with a pair potential obtained from an NPA local pseudopotential are unable to reproduce the experimental $S(k)$, showing a main peak displaced to the right of the experimental one [61].

The diffusion coefficient obtained is 0.55 Å^2 ps^{-1}, which is similar to the KS-AIMD result; however, there are no experimental data to compare with. Concerning the dynamic structure factor $S(k, \omega)$, we mention the recent IXS measurements performed by Scopigno *et al* [62], who report the quantum dynamic structure factor (which includes the detailed balance condition) not deconvoluted from the experimental resolution function. In order to compare our classical OF-AIMD $S(k, \omega)$ with the experimental ones, we have convoluted them with the resolution function and applied the correction due to detailed balance [62]. The comparison is shown in figure 6. The general shape of $S(k, \omega)$ is qualitatively well reproduced, for the three wave vectors considered. The central peak and the tails are well reproduced whereas some discrepancies appear as regards the positions of the side peaks, which appear at lower frequencies in the OF-AIMD simulations. In fact, the $S(k, \omega)$ show well defined peaks for k-values up to approximately 1.6 Å^{-1}, which is around 3/5 of k_p, a limit similar to that

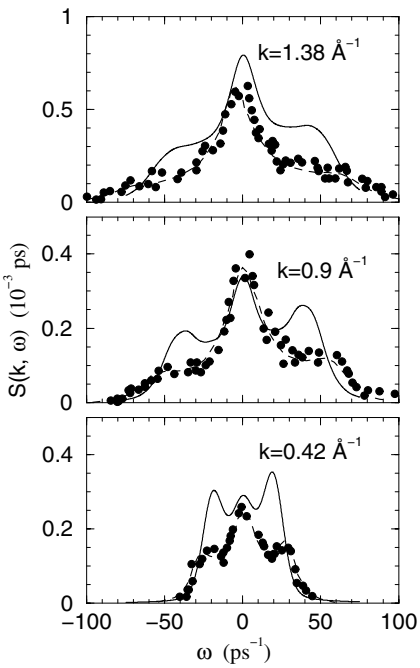

Figure 6. Quantum dynamic structure factors of liquid Al. Symbols and dashed lines: IXS results and experimental fits (k-values shown on the graphs). Full line: OF-AIMD results ($k = 0.40$, 0.98, and 1.44 Å^{-1}).

found for other liquid metals. The dispersion relation is plotted in figure 3. On extrapolating the OF-AIMD structure factor to $k = 0$ and taking the experimental value $\gamma = 1.25$ into account [63], the OF-AIMD adiabatic sound velocity is 4850 m s^{-1}, in good agreement with the experimental one, namely 4800 m s^{-1}. Figure 3 shows a positive dispersion, as in the case of liquid Li; a similar behaviour, though more marked, is also exhibited by the IXS data of Scopigno *et al* [62] with a maximum at about 0.45 Å^{-1}.

5.4. Liquid LiNa

The Li–Na liquid alloy has attracted much attention because it is a typical phase-separating system. The phase diagram is dominated by a region of two immiscible liquids and the phase-separation curve shows a consolute point located at $T \approx 577$ K and composition $x_{\mathrm{Li}} \approx 0.64$; this is close to the 'zero alloy' composition ($x_{\mathrm{Li}} \approx 0.61$) for which the total static structure factor, $S(k)$, reduces to the concentration–concentration partial structure factor $S_{cc}(k)$, i.e. $S(k) = S_{cc}(k)/x_{\mathrm{Li}}x_{\mathrm{Na}}$, because of the negative neutron scattering length of the ^{7}Li isotope. The total $S(k)$ has been measured for the zero alloy at several temperatures and also for other concentrations [64] while INS experiments have been performed for the zero alloy [65] only. At the zero alloy composition the experimental $S(k)$ are dominated by a strong small-angle scattering, which is a typical characteristic of a phase-separating system, and the oscillations of the $S(k)$ beyond the small-angle region are extremely small, with a characteristic ripple around $k \approx 2.2$Å^{-1}.

The simultaneous reproduction of the two features has been an objective since the very early theoretical and CMD simulations of the system [66–68], where either one of the features was obtained but the other was either absent (in the case of the double peak) or severely underestimated (in the case of the small-k divergency). Recently Canales *et al* [69] have succeeded in obtaining both features by using LRT-CMD with NPA pseudopotentials constructed *ab initio*. Also, they calculated the velocity autocorrelation functions and mean square displacements, leading to diffusion coefficients at $T = 590$ K with values $D_{\mathrm{Li}} = 1.18$ Å^2 ps^{-1} and $D_{\mathrm{Na}} = 1.28$ Å^2 ps^{-1}. The same NPA pseudopotentials have also been used by Anento *et al* [70] to study some dynamic properties by means of a simple theoretical model.

The zero alloy has also been investigated by means of KS-AIMD simulations. Hoshino and co-workers [71] used 100 atoms with an energy cut-off of 10 Ryd, and their $S(k)$ seems to reproduce the main experimental features, although the results are extremely noisy. Also, Costa Cabral and Martins [72] have used 108 atoms with an energy cut-off of 9 Ryd and similar non-local pseudopotentials, and the properties were obtained by averaging over 300–400 configurations. Their $S(k)$ qualitatively reproduces the experimental one, although quantitative differences appear over the whole k-region (see figure 7). They also report diffusion coefficients, $D_{\mathrm{Li}} = 0.80$ Å^2 ps^{-1} and $D_{\mathrm{Na}} = 0.91$ Å^2 ps^{-1}, which are somewhat lower than the LRT-CMD ones, but very similar to each other.

Here we present results of OF-AIMD simulations for the zero alloy at $T = 590$ K and $\rho = 0.032\,18$ Å^{-3}. The simulation was performed with 600 particles, the cut-off energy was 18 Ryd amounting to 84 500 plane-wave coefficients, and it lasted for 20 000 configurations (50 ps). Figure 7 shows the Bhatia–Thornton partial structure factors obtained (number–number $S_{NN}(k)$, concentration–concentration $S_{cc}(k)$, and number–concentration $S_{Nc}(k)$), and the total neutron weighted structure factor $S(k)$. For comparison, we include the LRT-CMD results of Canales *et al* [69] and the KS-AIMD results of Costa Cabral and Martins [72] along with the experimental data. The present results show an excellent agreement with experiment, improving on the KS-AIMD results and also the already good LRT-CMD results.

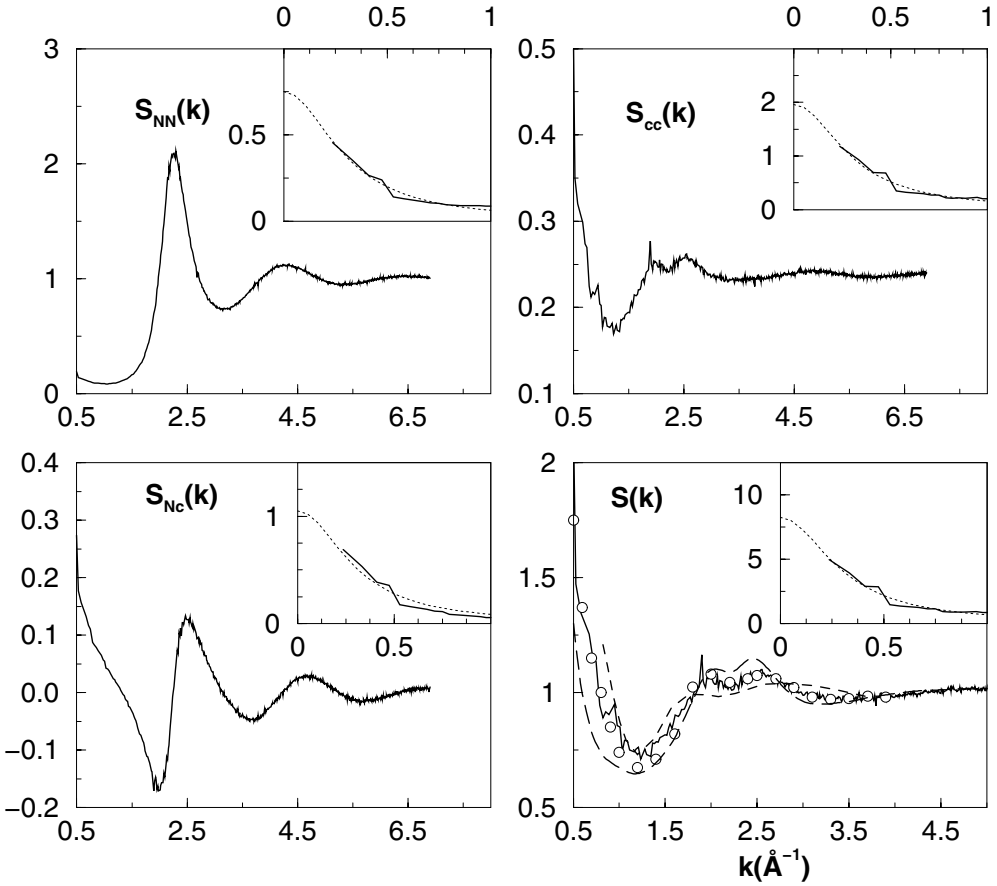

Figure 7. Bhatia–Thornton partial structure factors and total neutron weighted structure factors of liquid $Li_{0.61}Na_{0.39}$ at $T = 590$ K. Full lines: OF-AIMD results. Open circles: experimental neutron diffraction data. Dashed line: KS-AIMD results [72]. Long-dashed line: LRT-CMD results [69]. The insets show the low-k behaviour (full lines) and the extrapolation to $k = 0$ (dotted lines).

The insets show an extrapolation of the data to $k = 0$, obtained by assuming an Ornstein–Zernike formula of the type $S_{\alpha\beta}(k) = S_{\alpha\beta}(0)/(1 + \xi^2 k^2)$. The values obtained from the fits were $S_{NN}(0) = 0.75$, $S_{Nc}(0) = 1.05$, $S_{cc}(0) = 1.96$, and $\xi = 3.33$ Å, which is about 1/8 of the side of the simulation box.

The values of the diffusion coefficients are $D_{\mathrm{Li}} = 1.22$ Å^2 ps^{-1} and $D_{\mathrm{Na}} = 1.15$ Å^2 ps^{-1}, which are similar to those derived from the LRT-CMD results of Canales *et al* [69], although now D_{Li} is slightly larger than D_{Na}. We have also computed the product of $S_{cc}(0)$ and the interdiffusion coefficient from the autocorrelation function of the concentration current [73], obtaining that $S_{cc}(0)D_{\mathrm{int}} = 0.44$ Å^2 ps^{-1}; when compared with Darken's semiempirical expression, $x_1x_2(x_2D_1+x_1D_2) = 0.28$ Å^2 ps^{-1}, it shows that interparticle velocity correlations, ignored in Darken's expression, are indeed important in this system. Using the value of $S_{cc}(0)$ previously obtained, we end up with $D_{\mathrm{int}} = 0.23$ Å^2 ps^{-1}.

Figure 8 shows, for several k-values, the OF-AIMD partial intermediate-scattering functions obtained along with the LRT-CMD results of Anento *et al* [70]. For all k-values, a marked diffusive behaviour is clearly observed and, superimposed on it, a weak oscillating

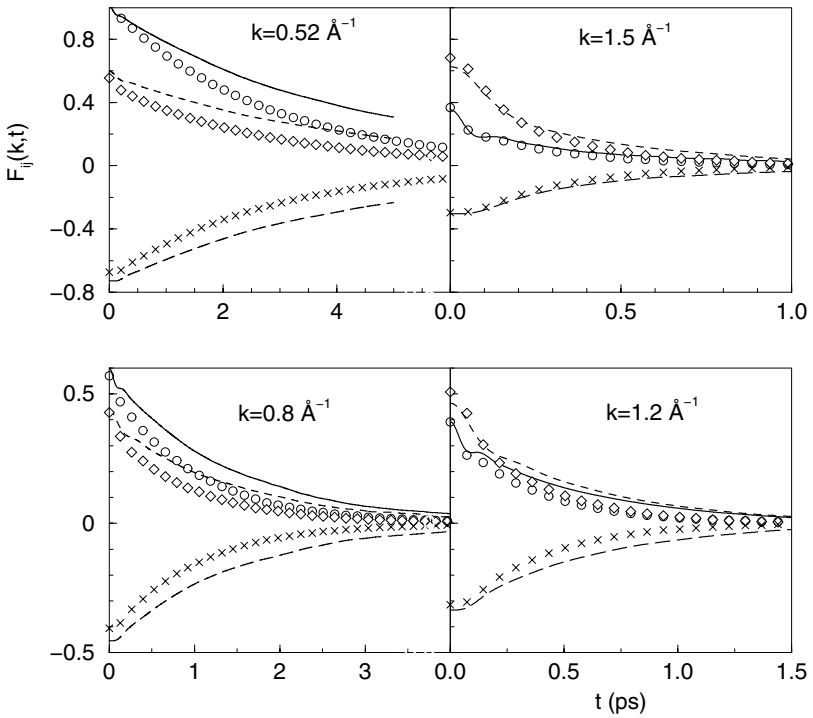

Figure 8. Partial intermediate-scattering functions of liquid $Li_{0.61}Na_{0.39}$ at $T = 590$ K. Lines: OF-AIMD results. Symbols: LRT-CMD data [70]. Full lines and circles: Li–Li partial. Dashed lines and diamonds: Na–Na partial. Long-dashed lines and crosses: Li–Na partial.

structure characteristic of a propagating mode. The decay of the functions is somewhat slower than in the LRT-CMD simulations, but the overall picture is the same. The partial dynamic structure factors obtained by Fourier transformation into the frequency domain confirm the appearance of peaks in $S_{\mathrm{LiLi}}(k,\omega)$ up to about 1.7 Å^{-1}, and in $S_{NN}(k,\omega)$ up to 1.4 Å^{-1} as already suggested by the LRT-CMD simulations [70]. On the other hand, both $S_{cc}(k,\omega)$ and the total neutron weighted $S_{\mathrm{tot}}(k,\omega)$ show a monotonic decay. In the hydrodynamic limit, the halfwidth at half-height of $S_{cc}(k,\omega)$ is given approximately by $D_{\mathrm{int}}k^2$, if coupling to temperature fluctuations is ignored [73]. In figure 9 we have plotted this halfwidth as a function of k^2 and we do indeed find that a linear regression is possible, but the slope takes the

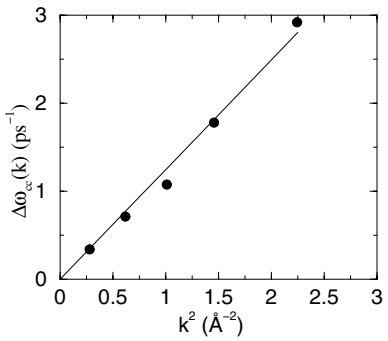

Figure 9. The halfwidth at half-maximum of $S_{cc}(k,\omega)$. Line: linear fit to the data.

value 1.24 Å^2 ps^{-1}, which is much larger than $D_{\rm int}$. This means that either the hydrodynamic regime has not yet been reached for the smallest k-value considered (0.52 Å^{-1}) or that coupling to temperature fluctuations is rather important for this alloy.

6. Conclusions

We have described how the dynamic properties of liquid metals can be evaluated starting from the pseudopotentials describing the interactions between valence electrons and ions. Moreover, the pseudopotentials can be constructed from first principles, using as input the atomic number and valence of the ions as well as the thermodynamic state of the system. The procedure is long and some approximations must be invoked, but in fact information on the static and dynamic properties can be obtained from the very basic atomic information. The essential approximation in the whole process is the calculation of the potential energy of the system. Linear response theory is a well established technique for liquid metals, and LRT-CMD simulations have been successfully applied to the study of many systems, although only recently has the LRT been combined with *ab initio* pseudopotentials (usually, model potentials were used). But LRT is a perturbative theory and therefore has limitations. Density functional theory provides a useful and more accurate alternative. In the Kohn–Sham formulation only the exchange–correlation energy has to be approximated, whereas in the orbital-free formulation, an (approximate) expression for the kinetic energy must be supplied too. However, as shown in this paper, the orbital-free representation allows a wider study of dynamical properties of different systems. We have focused on molecular dynamics techniques in order to obtain the static and dynamic properties of the liquid, but theoretical approaches also exist such as the mode-coupling theories developed recently [5, 74].

We stress that according to our view, the construction of the pseudopotential is closely connected with the theoretical framework used for the calculation of the potential energy of the system. This means that different kinetic energy functionals will lead to different pseudopotentials, even if they are developed from the same atomic pseudized valence properties. Concerning the results presented in this paper, we stress the reasonable agreement with the available experimental data, although some discrepancies remain. For instance, the positive dispersion relation of liquid Al is underestimated relative to the experimental results. Nevertheless, these results are rather promising and should prompt the development of more accurate kinetic energy functionals (which would lead to somewhat different pseudopotentials).

We end by remarking that the field of pseudopotential construction is, in fact, far from closed. We have seen that improvements are possible within the OF-DFT framework, which forces the use of local pseudopotentials. However, even the construction of non-local pseudopotentials remains open, at least regarding the calculation of dynamic properties of liquids, as is shown by the factor-of-300 error in the description of $S(k, \omega)$ for liquid Li for small k obtained in the KS-AIMD simulations, even though $S(k)$ is accurately reproduced.

Acknowledgments

This paper is dedicated to the memory of Dr Peter Verkerk and Dr Marta Alvarez, both participants of the Euroschool, who sadly died in a traffic accident shortly after it took place. All of us who knew them will miss their scientific contributions as well as their friendly and cheerful personalities.

We are grateful to M M G Alemany for sending us data prior to publication. This work was supported by Junta de Castilla y León (VA70/99) and DGES (PB98-0641-C02-01).

References

[1] Phillips J C and Kleinman L 1959 *Phys. Rev.* **116** 287
See also Harrison W A 1966 *Pseudopotentials in the Theory of Metals* (Reading, MA: Benjamin)
Heine V, Cohen M L and Weaire D 1970 *Solid State Physics* vol 24, ed H Ehrenreich, F Seitz and D Turnbull (New York: Academic)
[2] Heine V and Abarenkov I 1964 *Phil. Mag.* **9** 451
Abarenkov I V and Heine V 1965 *Phil. Mag.* **12** 529
[3] Shaw R W 1968 *Phys. Rev.* **174** 769
[4] Allen M P and Tildesley D J 1987 *Computer Simulation of Liquids* (Oxford: Clarendon)
[5] Balucani U and Zoppi M 1994 *Dynamics of the Liquid State* (Oxford: Clarendon)
[6] Torcini A, Balucani U, de Jong P H K and Verkerk P 1995 *Phys. Rev.* E **51** 3126
Casas J, González D J, González L E, Alemany M M G and Gallego L J 2000 *Phys. Rev.* B **62** 257
[7] Copley J R D and Rowe J M 1974 *Phys. Rev.* A **9** 1656
[8] Rahman A 1974 *Phys. Rev.* A **9** 1667
[9] Verlet L 1967 *Phys. Rev.* **159** 98
[10] Rasolt M and Taylor R 1975 *Phys. Rev.* B **11** 2717
[11] Dagens L, Rasolt M and Taylor R 1975 *Phys. Rev.* B **11** 2726
[12] Hohenberg P and Kohn W 1964 *Phys. Rev.* **136** B864
March N H and Lundquist S (ed) 1983 *Theory of the Inhomogeneous Electron Gas* (New York: Plenum)
[13] Ceperley D M and Alder B J 1980 *Phys. Rev. Lett.* **45** 566
[14] Vosko S H, Wilk L and Nussair M 1980 *Can. J. Phys.* **58** 1200
[15] Perdew J P and Zunger A 1981 *Phys. Rev.* B **23** 5048
[16] Alvarellos J E, Tarazona P and Chacón E 1986 *Phys. Rev.* B **33** 6579
[17] Alonso J A and Girifalco L A 1978 *Phys. Rev.* B **17** 3735
[18] Perdew J P 1991 *Electronic Structure of Solids '91* ed P Ziesche and H Eschrig (Berlin: Akademie) p 11
[19] Kohn W and Sham L J 1965 *Phys. Rev.* **140** A1133
[20] Kryachko E S and Ludeña E V 1990 *Energy Density Functional Theory of Many-Electron Systems* (London: Kluwer Academic) and references therein
[21] See Ashcroft N W and Mermin N D 1976 *Solid State Physics* (Philadelphia, PA: Holt-Saunders)
[22] Perrot F 1994 *J. Phys.: Condens. Matter* **6** 431
[23] Pearson M, Smargiassi E and Madden P A 1993 *J. Phys.: Condens. Matter* **5** 3221
Smargiassi E and Madden P A 1994 *Phys. Rev.* B **49** 5220
[24] Foley M and Madden P A 1996 *Phys. Rev.* B **53** 10 589
[25] Wang Y A, Govind N and Carter E A 1998 *Phys. Rev.* B **58** 13 465
Wang Y A, Govind N and Carter E A 1999 *Phys. Rev.* B **60** 16 350
[26] Chacón E, Alvarellos J E and Tarazona P 1985 *Phys. Rev.* B **32** 7868
[27] García González P, Alvarellos J E and Chacón E 1996 *Phys. Rev.* B **53** 9509
García González P, Alvarellos J E and Chacón E 1996 *Phys. Rev.* B **54** 1897
García González P, Alvarellos J E and Chacón E 1998 *Phys. Rev.* B **57** 4857
[28] González D J, González L E, López J M and Stott M J 2001 to be published
[29] Car R and Parrinello M 1985 *Phys. Rev. Lett.* **55** 2471
[30] Pastore G, Smargiassi E and Buda F 1991 *Phys. Rev.* A **44** 6334
[31] Foley M, Smargiassi E and Madden P A 1994 *J. Phys.: Condens. Matter* **6** 5231
[32] de Wijs G A, Pastore G, Selloni A and van der Lugt W 1995 *Phys. Rev. Lett.* **75** 4480
[33] Kresse G 1996 *J. Non-Cryst. Solids* **205–207** 833
[34] Anta J A and Madden P A 1999 *J. Phys.: Condens. Matter* **11** 6099
[35] Ashcroft N W 1966 *Phys. Lett.* **23** 48
[36] Fiolhais C, Perdew J P, Armster S Q and MacLaren J M 1995 *Phys. Rev.* B **51** 14 001
Fiolhais C, Perdew J P, Armster S Q and MacLaren J M 1996 *Phys. Rev.* B **53** 13 193
[37] Hamann D R, Schlüter M and Chiang C 1979 *Phys. Rev. Lett.* **43** 1494
Bachelet G B, Hamann D R and Schlüter M 1982 *Phys. Rev.* B **26** 4199
Hamann D R 1989 *Phys. Rev.* B **40** 2980
[38] Trouiller N and Martins J L 1991 *Phys. Rev.* B **43** 1993
[39] González L E, Meyer A, Iñiguez M P, González D J and Silbert M 1993 *Phys. Rev.* E **47** 4120
[40] de Jong P H K, Verkerk P and de Graaf L A 1994 *J. Phys.: Condens. Matter* **6** 8391
de Jong P H K, Verkerk P and de Graaf L A 1993 *J. Non-Cryst. Solids* **156** 48
[41] Sinn H, Sette F, Bergmann U, Halcoussis Ch, Krisch M, Verbeni R and Burkel E 1997 *Phys. Rev. Lett.* **78** 1715

[42] Scopigno T, Balucani U, Ruocco G and Sette F 2000 *J. Phys.: Condens. Matter* **12** 8009
[43] González L E, González D J, Silbert M and Alonso J A 1993 *J. Phys.: Condens. Matter* **5** 4283
[44] Olbrich H, Ruppersberg H and Steeb S 1983 *Z. Naturf.* a **38** 1328
[45] González D J, González L E and Hoshino K 1994 *J. Phys.: Condens. Matter* **6** 3849
[46] Canales M, Padró J A, González L E and Giró A 1993 *J. Phys.: Condens. Matter* **5** 3095
Canales M, González L E and Padró J A 1994 *Phys. Rev.* E **50** 3656
[47] Vanderbilt D 1990 *Phys. Rev.* B **41** 7892
[48] Waseda Y 1980 *The Structure of Non-Crystalline Materials* (New York: McGraw-Hill)
IAMP Database of SCM-LIQ Tohoku University, URL: http://www.iamp.tohoku.ac.jp/database/scm/LIQ
[49] Hornung K 1985 *Handbook of Thermodynamic and Transport Properties of Alkali Metals* ed R W Ohse (Oxford: Blackwell) ch 6.4
[50] Murday J S and Cotts R M 1971 *Z. Naturf.* a **26** 85
Gerl M and Bruson A 1985 *Handbook of Thermodynamic and Transport Properties of Alkali Metals* ed R W Ohse (Oxford: Blackwell) ch 7.5
[51] Pilgrim W-C, Hosokawa S, Saggau H, Sinn H and Burkel E 1999 *J. Non-Cryst. Solids* **250–252** 96
[52] Pasqualini D, Vallauri R, Demmel F, Morkel C and Balucani U 1999 *J. Non-Cryst. Solids* **250–252** 76
[53] Bodensteiner T, Morkel C, Glaser W and Dorner B 1992 *Phys. Rev.* A **45** 7509
[54] Alemany M M G, Casas J, Rey C, González L E and Gallego L J 1997 *Phys. Rev.* E **56** 6818
[55] Alemany M M G 2000 private communication
[56] Anta J A, Jesson B J and Madden P A 1998 *Phys. Rev.* B **58** 6124
[57] Jacucci G, Taylor R, Tenenbaum A and van Doan N 1981 *J. Phys. F: Met. Phys.* **11** 783
[58] Hafner J and Jank W 1990 *Phys. Rev.* A **42** 11 530
Ebbsjo I, Kinell T and Waller J 1980 *J. Phys. C: Solid State Phys.* **13** 1865
[59] Blochl P E and Parrinello M 1992 *Phys. Rev.* B **45** 9413
[60] Takeda S, Harada S, Tamaki S and Waseda Y 1991 *J. Phys. Soc. Japan* **60** 2241
[61] González L E and González D J 2000 unpublished
[62] Scopigno T, Balucani U, Ruocco G and Sette F 2000 *Phys. Rev.* E **63** 011210
[63] Webber G M B and Stephens R W B 1968 *Physical Acoustics* vol IVB, ed W P Mason (New York: Academic)
[64] Ruppersberg H and Knoll W 1977 *Z. Naturf.* a **32** 1374
[65] Gartrell-Mills P R, McGreevy R L and van der Lugt W 1988 *Physica* B **154** 1
[66] Hoshino K and Young W H 1986 *J. Phys. F: Met. Phys.* **16** 1671
González D J and Silbert M 1988 *J. Phys. F: Met. Phys.* **18** 2353
Hafner J and Jank W 1988 *J. Phys. F: Met. Phys.* **18** 333
[67] Hoshino K, Silbert M, Stafford A and Young W H 1987 *J. Phys. F: Met. Phys.* **17** L49
Hoshino K and van Wering J J 1988 *J. Phys. F: Met. Phys.* **18** L23
[68] Mori H, Hoshino K and Watabe M 1992 *J. Phys. Soc. Japan* **61** 1218
[69] Canales M, González D J, González L E and Padró J A 1998 *Phys. Rev.* E **58** 4747
[70] Anento N, Casas J, Canales M, González D J, González L E and Padró J A 1999 *J. Non-Cryst. Solids* **250–252** 348
[71] Senda Y, Shimojo F and Hoshino K 1998 *J. Phys. Soc. Japan* **67** 2753
[72] Costa Cabral B J and Martins J L 1999 *J. Chem. Phys.* **111** 5067
[73] Hansen J-P and McDonald I R 1986 *Theory of Simple Liquids* (London: Academic)
[74] Sjölander A 1987 *Amorphous and Liquid Materials* ed E Lüscher, G Fritsch and G Jacucci (Dordrecht: Nijhoff)
Sjögren L and Sjölander A 1979 *J. Phys. C: Solid State Phys.* **12** 4369